Flowfield Measurements Inside a Boundary-Layer Bleed Slot

D. O. Davis,* B. P. Willis,† and W. R. Hingst†
NASA Lewis Research Center, Cleveland, Ohio 44135

An experimental investigation was conducted to determine the flowfield inside a bleed slot used to control an oblique shock-wave and turbulent boundary-layer interaction. The slot was oriented normal to the primary flow direction and had a width of 1.0 cm (primary flow direction) and a length of 2.54 cm and spanned 16.5 cm. The approach boundary layer upstream of the interaction was nominally 3.0 cm thick. Two operating conditions were studied: $M = 1.98$ with a shock generator deflection angle of 6 deg and $M = 2.46$ with a shock generator deflection angle of 8 deg. Measurements include surface and flowfield static pressure, pitot pressure, and total mass flow through the slot. The results show that despite an initially two-dimensional interaction for the zero-bleed-flow case, the slot does not remove mass uniformly in the spanwise direction. Inside the slot, the flow is characterized by two separation regions, which significantly reduce the effective flow area. The upper separation region acts as an aerodynamic throat, resulting in supersonic flow through much of the slot.

Nomenclature

B	= bias uncertainty
B_c	= correlated bias uncertainty
C_f	= friction coefficient
D_x	= slot width (Fig. 2)
D_z	= slot span (Fig. 3)
L	= slot length (Fig. 2)
M	= Mach number
$\dot{m}$	= mass-flow rate
$\dot{m}'_{bl}$	= unit boundary-layer mass-flow rate, $\rho_e U_e (\delta - \delta^*)$
$\bar{\dot{m}}$	= normalized mass-flow rate [Eq. (2)]
P	= static pressure
P_t	= total pressure
P_{t2}	= pitot pressure
$\bar{P}_w$	= normalized wall static pressure [Eq. (3)]
Q	= sonic flow coefficient [Eq. (1)]
Re	= unit Reynolds number, $\rho_e U_e / \mu_e$
S	= precision uncertainty
T_t	= total temperature
U, V, W	= mean velocity components in the x, y, z directions, respectively
U_M	= uncertainty in Mach number
x, y, z	= Cartesian coordinate system
α	= shock generator deflection angle (Fig. 2)
γ	= ratio of specific heats, $\gamma = 1.4$ for air
δ	= boundary-layer thickness
δ^*	= displacement thickness
θ	= momentum thickness
μ	= viscosity
ρ	= density

Subscripts

cl	= centerline condition
e	= boundary-layer edge condition
i	= inviscid condition
plen	= condition in bleed plenum
ref	= condition in upstream reference plane
w	= condition at wall
0	= condition in wind-tunnel plenum
1, 2, 3	= conditions in zones 1, 2, and 3, respectively (Fig. 2)

Introduction

PREVENTION or control of boundary-layer separation resulting from a shock-wave and boundary-layer interaction can be achieved by removing low momentum fluid (boundary-layer mass) near the surface through a porous region.[1,2] The porous region may be a series of discrete perforations (holes) or a single slot. Numerical analysis of the interaction region can be very costly in terms of computer time and grid generation if the flow through the individual holes or the slot is endeavored. This is especially true if the interaction is part of a full supersonic inlet calculation. To avoid this, a global bleed model is sought that eliminates the need for resolving the bleed-flow passages. An effective global bleed model should do two things: predict the amount of mass removed from the boundary layer and predict the condition of the boundary layer downstream of the interaction. The former is important from the standpoint of bleed drag and bleed system scaling, whereas the latter is an indication of the effectiveness of the bleed in maintaining a healthy boundary layer. To achieve these goals, the local flow phenomena in the interaction region, including the bleed passages and bleed plenum, must be understood and accounted for in a model. Not surprisingly, previous investigations resolving the flow through bleed passages have been computational in nature. Hamed et al. studied the oblique shock-wave and laminar boundary-layer interaction with bleed through normal slots[3] and the oblique shock-wave and turbulent boundary-layer interaction with bleed through various normal[4-6] and slanted[5,7] slots. Because the slot configuration is two dimensional, Hamed et al. were able to perform a fairly comprehensive parametric study, including the effects of bleed mass-flow rates, slot location relative to shock impingement location, slot inclination angle, and slot length-to-width ratio. Hahn et al.[8] also numerically studied the oblique shock-wave and turbulent boundary-layer interaction with bleed through normal slots and, in addition to investigating various shock impingement locations and slot length-to-width ratios, included the effects of two slots with various streamwise spacing. Other researchers[9-12] considered the more complex (three-dimensional) case of oblique shock-wave and turbulent boundary-layer interactions with bleed through holes. These numerical studies identified several important features of the bleed interaction. Among them are the presence of separation region(s) in the bleed passage, which have a large effect on the flow coefficient of the hole or slot,[13] and the presence of a two-segment barrier shock (see Fig. 1), which may or may not be attached, depending on local flow conditions. Although these studies provide a significant increase in the

Fig. 1   Schematic of bleed interaction region (no scale).

Table 1   Wind-tunnel operating conditions

Operating conditions	M_{ref}	
	1.98	2.46
$P_{t,0}$ kPa	138.0	172.4
$T_{t,0}$ °K	293.0	293.0
$Re_{ref} \times 10^{-7}$ /m	1.77	1.75
δ_{ref} cm	2.62	3.06
δ^{*}_{ref} cm	0.565	0.712
θ_{ref} cm	0.201	0.196
$C_{f,ref} \times 10^{3}$	1.50	1.29
$\dot{m}'_{bl,ref}$ kg · s^{-1} · cm^{-1}	0.04047	0.03768

Fig. 2   Slot bleed experiment schematic.

understanding of the shock-wave and boundary-layer interaction with bleed, unfortunately there have been no experimental flowfield data with which to compare. The present experimental investigation was undertaken to gain further insight into the slot-bled oblique shock-wave and turbulent boundary-layer interaction and to provide validation data for computational fluid dynamics (CFD) methods.[6]

Experimental Program

A schematic of the slot bleed experiment with reference coordinates is shown in Figs. 2 and 3. The bleed model is a single 90-deg slot, 1.00 cm wide (D_x) and 2.54 cm long (L), as shown in Fig. 2, and spanning 16.51 cm (D_z), as shown in Fig. 3. As indicated in Fig. 2, an oblique shock wave is generated by a rotatable and translatable (x direction) sharp-edged plate (shock generator). The shock generator spans the full width (30.5 cm) of the wind tunnel. For a given deflection angle α, the shock generator is translated until an inviscid shock wave originating at the generator leading edge will impinge on the upstream edge of the slot. To the axial position of the shock generator, the inviscid shock angle β is calculated on the basis of the core Mach number measured in the upstream reference plane indicated in Fig. 2. Boundary-layer fences were used to isolate the wind-tunnel test section corner flow from the interaction region.

The experiments were performed in the NASA Lewis Research Center 1 × 1 ft supersonic wind tunnel (SWT), which is a continuous-flow facility with Mach number variation provided by replaceable nozzle blocks. A schematic of the 1 × 1 SWT experiment is shown in Fig. 4. The approach boundary layer is the naturally occurring boundary layer on the wind-tunnel wall. The oblique shock wave interacts with the boundary layer, and a portion of the resulting distorted boundary layer is removed through the bleed slot. The bleed flow exhausts into a large plenum where the plenum static pressure is recorded. The bleed flow rate was measured with calibrated American Society of Mechanical Engineers (ASME) nozzles, and the rate of mass flow was controlled by a choked mass-flow plug.

Fig. 3   Plan view of slot bleed experiment.

Fig. 4   Slot bleed experiment wind-tunnel schematic.

Bleed vacuum was supplied by lab-wide altitude exhaust and a 450-psi air ejector system.

Data were obtained for two wind-tunnel operating conditions. These conditions are referred to by the wind-tunnel core Mach number measured in the upstream reference plane (see Fig. 2). Table 1 summarizes the wind-tunnel plenum condition and the boundary-layer characteristics measured in the reference plane for each of the reference Mach numbers. The unit Reynolds number reported in this table is based on the total conditions in the wind-tunnel plenum and the core Mach number in the reference plane (M_{ref}). For the $M_{ref} = 1.98$ condition, the shock-generator deflection angle was set at $\alpha = 6$ deg, and for the $M_{ref} = 2.46$ condition, the deflection angle was set at $\alpha = 8$ deg. Previous experience[14] has shown that for both cases the shock strength is sufficient to separate the wind-tunnel boundary layer. Hereafter, the two cases are referred to by the M198A6 and M246A8 designations.

Instrumentation

The experiment was instrumented to measure surface and flow-field static pressure, flowfield pitot pressure, and the total mass flow through the slot. All flowfield measurements were made in the $z = 0$ plane of symmetry, using conventional (intrusive) pressure probes. Because it was recognized that there would be large gradients and flow angles in the slot, efforts were made to choose instrumentation least sensitive to these conditions. However, as with all forms of intrusive-type probes, inherent errors are introduced into the measurements, which are very difficult to quantify. Regions of the flow that the authors believe to have a high level of uncertainty are accordingly identified.

All pressures were measured with a Pressure Systems Incorporated electronically scanned pressure system using ± 5-psid range transducers. The transducer precision uncertainty S, transducer bias uncertainty B, and correlated bias errors between transducers, B_c, were estimated using Blumenthal's personal computer program[15] and are $S = 0.0230$, $B = 0.0150$, and $B_c = 0.0136$ (kPa).

Surface static-pressure data were measured with pressure-sensitive paint and with conventional static-pressure taps. The pressure-sensitive paint data were acquired using the technique described by Bencic.[16]

Flowfield static-pressure data were measured using a knife-edged probe, as shown in Fig. 5. To measure flowfield static pressure, a special bleed-plate insert was fabricated that had small grooves machined along the vertical interior surfaces of the slot on the centerline as shown in the inset of Fig. 5. These grooves serve as a guide for the knife-edged probe. Five 0.254-mm-diam static-pressure taps are located on a 0.254-mm-thick sharp-edged brass shim. The taps are offset from the slot centerline such that a reversal (180-deg rotation about the stem) of the probe in the guides will yield data between the original tap positions for a total of 10 data points in the x direction.
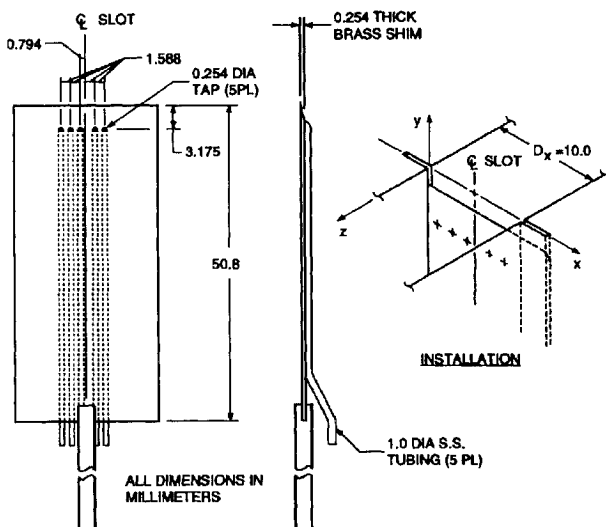

Fig. 5   Knife-edged static-pressure probe detail.

The probe was zeroed with the center of the taps lying in the $y = 0$ plane (wind-tunnel surface). A remotely controlled actuator in the bleed plenum then pulled the probe through the slot. Knife-edged probes are known to be very sensitive to yaw misalignment.[17] However, because all of the data taken were confined to the plane of symmetry and the machined guides prevented aerodynamic deflection of the probe, the errors attributable to yaw misalignment were minimized.

Pitot pressure measurements were made with a 0.508-mm-diam square-edged round pitot tube probe having an inner-to-outer diameter ratio of 0.4. Based on data presented by Bryer and Pankhurst,[17] the critical angle for this probe configuration is ± 15 deg for incompressible flow and slightly larger for supersonic flow. Calibration of the probe in a Mach 2.0 stream showed that the probe would read within 2% of the actual pitot pressure for pitch angles as high as ± 20 deg. The probe was actuated from within the bleed plenum in the x and y direction.

The total mass flow through the slot was measured with an ASME flow nozzle. The flow rate is determined from a semiempirical relation that gives the mass flow as a function of nozzle geometry, temperature, upstream pressure, and the pressure drop across the nozzle. A description and uncertainty analysis of this system is given by Willis et al.[18] For the present measurements, the uncertainty is estimated to be $\pm 2.20\%$ of the calculated mass flow.

Results and Discussion

Comparison of the results for the M198A6 and M246A8 cases revealed qualitative similarities. Therefore, in the following sections, most of the results presented are for the M246A8 case. The corresponding figures for the M198A6 cases can be found elsewhere.[19]

Sonic Flow Coefficient

Numerical simulations of a bleed region utilizing a global bleed model must specify the bleed mass flow, which usually varies with local flow conditions, as a boundary condition. The mass flow may be determined from semiempirical relations or from an experimental table look-up for a given bleed configuration. The ability of a bleed configuration to remove mass from the boundary-layer is typically quantified by the sonic-flow coefficient:

$$Q = \frac{\dot{m}}{\dot{m}_{ideal,choked}} \tag{1}$$

which is usually presented as a function of the ratio of bleed plenum static pressure to freestream total pressure. Sonic-flow-coefficient distributions were measured for the case of an undistorted-approach boundary layer ($\alpha = 0$ deg) for four reference Mach numbers and are shown in Fig. 6. These data are presented here for reference and can be used to validate flow coefficient models for use in CFD methods. A comprehensive discussion of flow coefficient behavior for the present slot and other bleed configurations is given by Willis et al.[18]

When an oblique shock wave is positioned upstream of the slot, the local Mach number in the vicinity of the slot is reduced from the upstream reference value, and a shift to a different flow coefficient curve occurs. An interesting feature in Fig. 6 is the presence of a distinct kink in all of the flow coefficient distributions. This is the location where choked flow occurs in the slot. The effective throat area, however, is determined by the size of the separation region (see Fig. 1), which can vary with local flow conditions. Lowering the plenum pressure below this choke point causes an increase in effective throat area, and more mass is passed through the slot.

Surface Static Pressure

Pressure-sensitive paint was applied to the bleed-plate insert shown in Fig. 3. Initially, it was thought that, with the boundary-layer fences and the relatively large span-to-width ratio ($D_z/D_x = 16.5$) of the slot, the interaction near the center of the slot would be nearly two-dimensional. For the case of no bleed flow, this was indeed the case. However, when the bleed flow was nonzero, the interaction became more three-dimensional. This behavior is illustrated by the surface static pressure obtained with the pressure-sensitive paint and is shown in Figs. 7 and 8 for the M198A6 and M246A8 cases, respectively. In these figures, the lower half of the plot corresponds to
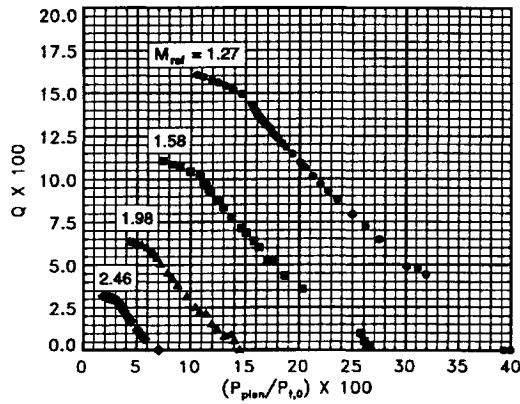
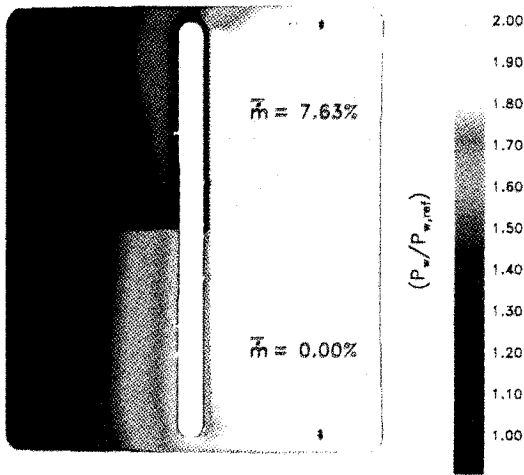**Fig. 6 Sonic-flow coefficient distributions, $\alpha = 0$.**

Fig. 7 Surface static pressure from pressure-sensitive paint, case M198A6.
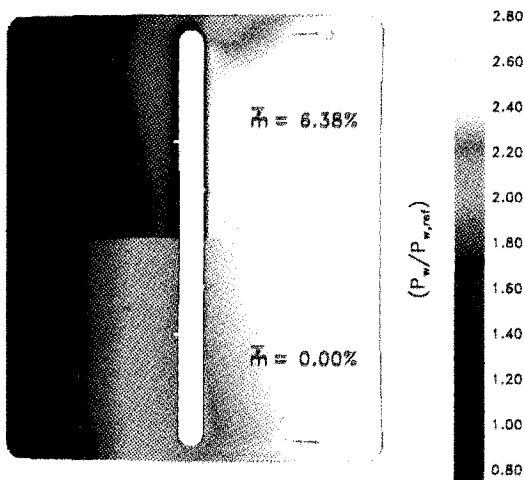

Fig. 8 Surface static pressure from pressure-sensitive paint, case M246A8.

the no-bleed case and the upper half corresponds to the highest bleed flow rate attainable with the bleed system. The bleed rates are given as a percentage of the mass flow in the approach boundary-layer defined as

$$\bar{m} = \frac{100 \cdot \dot{m}}{(D_z) \cdot (\dot{m}'_{\text{bl,ref}})} \qquad (2)$$

where $\dot{m}'_{\text{bl,ref}}$ is the unit boundary-layer mass flow in the upstream reference plane (see Table 1) and D_z is the spanwise dimension of the slot (see Fig. 3). Although the data for each flow rate are

shown for only half of the bleed plate, results were obtained across the entire plate and exhibited a high degree of symmetry about the wind-tunnel centerline ($z = 0$).

For the cases with no bleed flow (the lower half of Figs. 7 and 8), the results indicate a reasonably two-dimensional flowfield except in the vicinity of the slot ends. As the bleed flow rate is increased, the upstream influence of the shock wave decreases, but not uniformly across the span of the slot. At the center of the slot ($z = 0$), the upstream influence is significantly less than at the slot ends. This spanwise variation of upstream influence indicates that more mass flow is removed near the center of the slot. Although the interaction is not two-dimensional, the results were observed to be symmetric about the wind-tunnel centerline ($z = 0$ plane) and are still valid for a three-dimensional CFD validation case.

Conventional surface static taps were located axially on the wind-tunnel centerline through the interaction region. Normalized surface static-pressure distributions along the x axis (centerline) for three bleed rates are shown in Fig. 9 for the M246A8 case. The normalized wall pressure is defined as

$$\bar{P}_w = \frac{(P_w - P_{1,i})}{(P_{3,i} - P_{1,i})} \qquad (3)$$

where i denotes the inviscid no-bleed condition. In this plot, the symbols represent data from the conventional surface pressure taps and the solid lines represent data deduced from the pressure-sensitive paint. The theoretical inviscid distribution for the no-bleed case is also represented in this plot. The layout sketch at the top of Fig. 9 shows the inviscid no bleed wave structure. The three bleed rates shown represent the no-bleed case, the maximum bleed attainable for the configuration, and an arbitrary bleed rate between the two extremes.

From Fig. 9 and the corresponding figure for the M198A6 case (shown elsewhere[19]), the following observations can be made:

1) The upstream influence of the shock-wave and boundary-layer interaction is reduced by approximately 1.5 cm for the M198A6 case and by approximately 2.5 cm for the M246A8 case when bleed is applied.

2) For both cases, there is very little difference between the distributions corresponding to the two nonzero-bleed rates.

3) For the nonzero-bleed cases, the pressure overshoots the inviscid pressure distribution. This overshoot in pressure is attributed to the barrier shock (see Fig. 1) and, as expected, is greater for the higher-bleed-rate case.
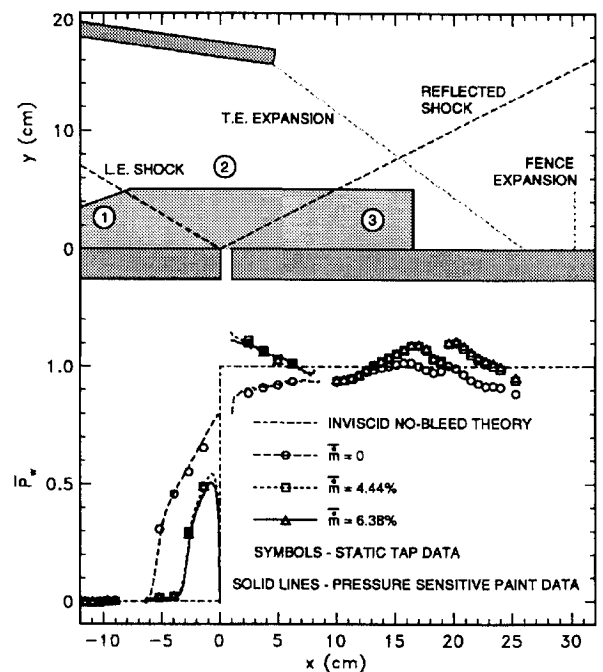

Fig. 9 Normalized surface static-pressure distributions along the x axis, case M246A8.

4) The pressure-sensitive paint data agree quite well with the conventional static tap data.

5) The drop in pressure below the inviscid value is attributable to the upstream influence of the expansion-wave system set up by the experimental hardware (shock generator and fences).

Flowfield Measurements in the Slot

For the flowfield measurements, only one bleed rate was considered for each of the two operating conditions. The bleed rate considered corresponds to the maximum attainable with the bleed system and is the same as the highest bleed rate condition reported for the surface static-pressure data. With reference to the sonic-flow-coefficient distributions (Fig. 6), for all local Mach numbers, the highest flow rate attainable with the bleed system is always to the left of the aforementioned choke point in the flow coefficient curves.

The knife-edged static probe was used to measure the static pressure in the slot. In Fig. 10, the normalized static pressure along the x axis (top of the slot) is plotted along with the surface static pressure upstream and downstream of the slot for the M246A8 case. From this figure, it is clear that the pressure distribution across the top of the slot is not uniform and follows the trends of the surface static pressure. The slot static-pressure distribution in the plane of symmetry, normalized by the wind-tunnel total pressure $(P_{t,0})$, is shown in Fig. 11 for the M246A8 case. A total of 210 points was measured on a regular grid with x and y spacing as indicated by the tick marks shown in Fig. 11. For presentation purposes, the data have been extrapolated to the slot surfaces by setting the pressure at the surface equal to the flowfield pressure at the first point away from the surface. The normalized bleed plenum static pressure is indicated on the bottom of the figure. Although undoubtedly smeared by the presence of the boundary-layer developing on the knife-edged static probe, the presence of the interior segment of the barrier shock is clearly seen by the large pressure gradient (increase) in the upper-right region of the flowfield. It is not clear, however, whether the shock is attached or not. Outside this region, the static pressure is fairly uniform throughout the slot.

A 0.508-mm-diam pitot probe was used to measure the pitot pressure in the slot. Normalized pitot pressure distributions for the M246A8 case are shown in Fig. 12. A total of 441 points was measured on a regular grid with x and y spacing, as indicated by the tick marks in Fig. 12. Near the top of the slot, very large flow angles relative to the pitot probe stem are expected, and the pitot data should be considered very uncertain. This probably accounts for the lack of a discrete barrier shock in the data. Also, note that the pitot probe will sense nearly static pressure in regions of reverse flow. These results indicate two fairly extensive regions of flow separation in the slot, which severely reduce the effective flow area. The data do indicate, however, that the flow reattaches before exiting into the bleed plenum.

The pitot and static pressure data were combined to calculate the local Mach number distribution in the slot, using the appropriate isentropic relations[19] with the ratio of specific heats specified as

Fig. 10   Normalized static-pressure distribution along the x axis, case M246A8, $\bar{m} = 6.38\%$.

$\gamma = 1.4$. For the calculation, the local static pressure P data were interpolated onto the data grid used to acquire the pitot data. Recall that the static pressure at the slot surface was set equal to the first column of data and recognize that this may introduce errors in the Mach number values nearest the slot surface. The calculated Mach number distributions for the M198A6 and M246A8 cases are shown in Figs. 13 and 14, respectively. The presence of the separation region on the upper-left surface of the slot causes an aerodynamic convergent–divergent nozzle effect. As the flow expands downstream of the aerodynamic throat, the Mach number increases to a peak of about $M = 2$ for both cases. The backpressure in the plenum, however, is not low enough to maintain supersonic flow. But rather than shocking down to subsonic flow, as would happen for the inviscid case, the plenum pressure feeds up through the boundary layer on the slot surface, which causes the flow to separate. Compression waves off of this separation act to decelerate the flow gradually but still the flow exits the slot supersonically. The upper separated region also leaves a rather large subsonic wake that accelerates to a near-sonic condition at the slot exit.

Following Coleman and Steele,[20] the propagation of the bias and precision uncertainties in the measured pitot and static pressures into the calculated Mach number were estimated. The overall uncertainty in the Mach number U_M, is then estimated by root-sum squaring (95% confidence) the bias and precision uncertainties.[19] The overall uncertainty in the Mach number was evaluated at each point in the flowfield, and the results are shown in Fig. 15 as a function of the local Mach number. Note that this Mach number uncertainty includes only the propagation of pressure measurement uncertainty and not errors attributable to probe interference, misalignment, or interpolation. The results indicate that the uncertainty becomes excessive for a local Mach number less than 0.5, which is confined to relatively small regions of the flowfield.

Three-Dimensionality of the Flowfield

From the surface static-pressure distributions (Figs. 7 and 8), we inferred that the mass-flow distribution in the spanwise (z) direction was not uniform, but passed a higher mass flow at the center of the slot. If we assume that the total temperature of the flow in the slot is the same as that of the wind-tunnel plenum, then in conjunction with the static-pressure and Mach number distributions in the slot, and assuming that the ideal gas law applies, we can calculate a mass-flux $(-\rho V)$ distribution in the slot. Integrating the $-\rho V$ distribution along lines of constant (y) locations and then dividing by the unit mass flow in the reference boundary layer yields a normalized mass flow in the plane of symmetry:

$$\bar{m}_{cl} = 100 \cdot \frac{\int_0^{D_x} -\rho V \, dx}{\dot{m}'_{bl,ref}} \qquad (4)$$

There are, however, at least three sources of errors to consider when performing the integration: regions of high flow angle relative to the pitot probe stem, regions of reverse flow, and regions where the static pressure has a high gradient near the wall, which makes our extrapolation assumption uncertain. The integrations were performed along 18 rows of data, and the results are shown in Fig. 16. In this plot, the centerline mass flow calculated from Eq. (4) is normalized by the bulk mass flow measured with the ASME nozzle and presented as a function of $-y$ location. Data near the top of the slot $(-y/D_x < 0.3)$ are omitted because of the expected large flow angles relative to the pitot probe. From this figure we can estimate that for the bulk mass flows considered, on the average the centerline mass flow is roughly 50% higher than the bulk mass flow. Also, the increase in centerline mass flow through the slot indicates a significant spanwise convergence of the flow within the slot.

With regard to the cause of the observed three-dimensionality of the flowfield, there are three geometric considerations: the bleed plenum, the boundary-layer fences, and the end effects of the slot itself. The bleed plenum is unlikely to be contributing to the nonuniform flow inasmuch as the spanwise dimension of the plenum (30 cm) is nearly twice the span of the slot (16.5 cm) and the depth of the plenum (60 cm) is approximately twice that of the span. More likely is that the nonuniform condition is attributable to a combination of the boundary-layer fences and slot end effects. Under
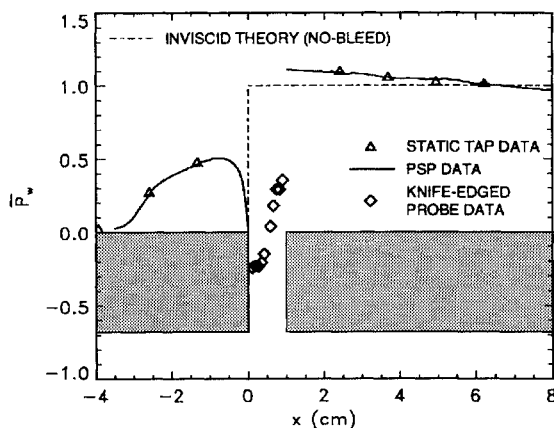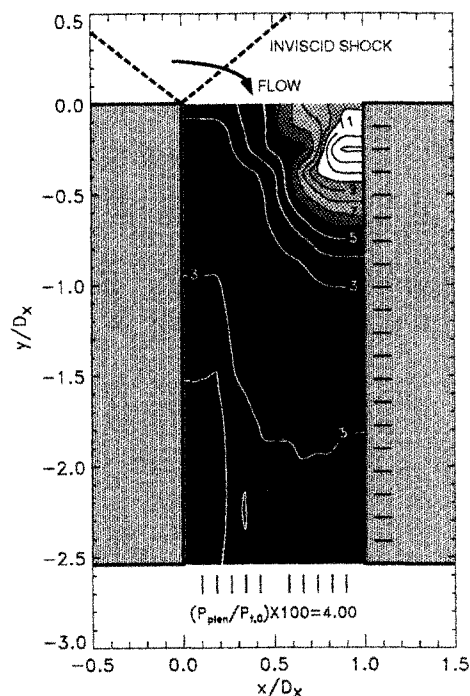
Fig. 11 Normalized static-pressure distribution [$(P/P_{t,0}) \times 100$], case M246A8, $\bar{m} = 6.38\%$.
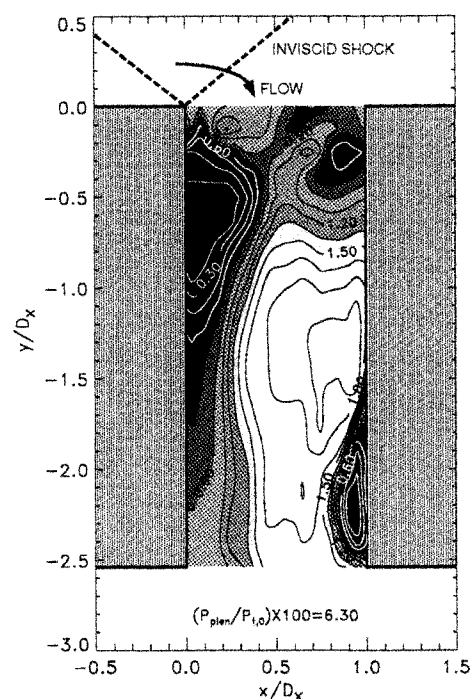

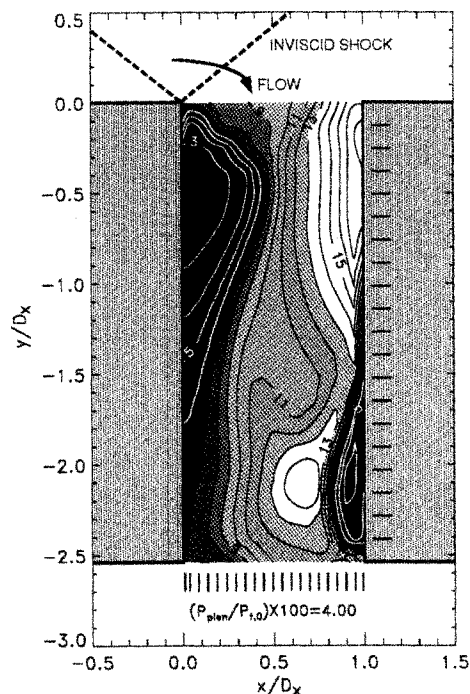**Fig. 13** Calculated Mach number distribution, case M198A6, $\bar{m} = 7.63\%$.

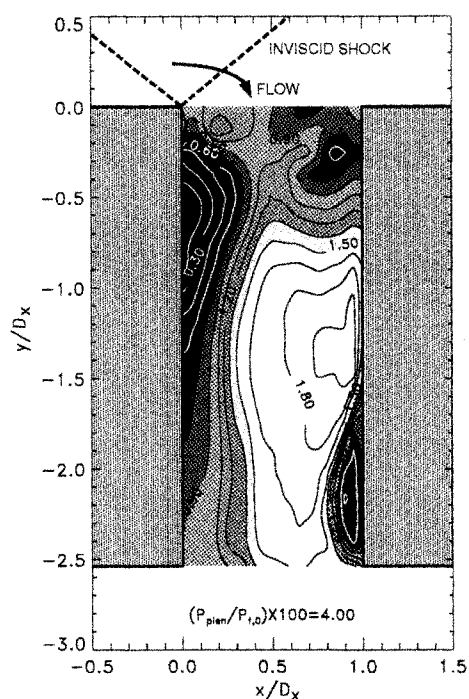**Fig. 12** Normalized pitot pressure distribution [$(P_{t2}/P_{t,0}) \times 100$], case M246A8, $\bar{m} = 6.38\%$.

Fig. 14 Calculated Mach number distribution, case M246A8, $\bar{m} = 6.38\%$.

no-bleed conditions, the oblique shock wave separates the wind-tunnel boundary layer nearly uniformly across most of the span of the wind-tunnel wall. The fence corner region, however, is more susceptible to separation because of the low momentum of the fluid in the corner. In addition, the glancing shock wave and boundary-layer interaction on the fence surface causes the flow separation to extend up the side of the fence. The result of the corner interaction is to locally turn the flow toward the wind-tunnel centerline. Removing the fences is not an option, however, because previous experience has shown that the separation of the much thicker wind-tunnel corner boundary layer prevents spanwise uniformity for all bleed conditions, zero or otherwise. When bleed is applied to the

fenced configuration, the separation in the vicinity of the fence corner is not affected by the bleed as much as at the centerline because the slot does not extend all the way to the fence. The result is that the nominally two-dimensional no-bleed separation becomes three-dimensional, significantly affecting the local bleed flow rate through the slot. The above conjectured behavior has been supported by surface oil flow visualization, which shows very large flow angles (~45 deg) converging toward the centerline in the vicinity of the corners under bleed and no-bleed conditions. However, further experimental data in conjunction with CFD analysis likely will be required to fully understand this complex interaction. Extending the slot fully to the corner and perhaps increasing the slot area locally in the
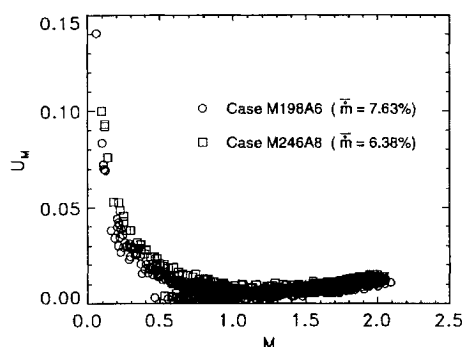
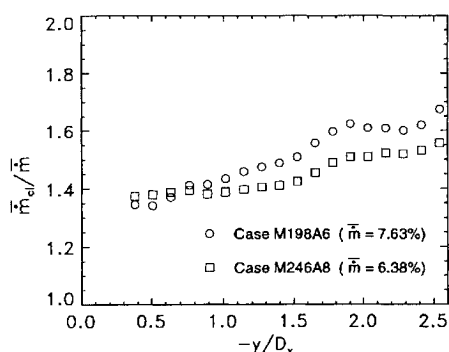**Fig. 15   Uncertainty in Mach number vs Mach number.**

Fig. 16   Integrated mass flow in the plane of symmetry.

corner may alleviate the problem and will be the subject of a future investigation.

Concluding Remarks

Development of global bleed models for boundary-layer control will require experimental and computational synergism because of the complexity of the flowfield. The flowfield inside a bleed slot used to control an oblique shock-wave and turbulent boundary-layer interaction has been studied experimentally. From this study we can draw the following conclusions:

1) For the configuration tested, despite a nominally two-dimensional flowfield for the zero-bleed case, application of bleed flow resulted in a highly three-dimensional flowfield. Surface static-pressure data and local mass-flow calculations indicate that the slot passes significantly more mass flow near the center than at the ends. This may very well be the case in actual inlet bleed systems.

2) The flowfield in the plane of symmetry of the slot is characterized by the presence of a barrier shock and two large separation regions. These features serve to reduce the flow coefficient of the bleed passage, and their effects should be included in flow coefficient models.

3) Because of an aerodynamic throat effect of the separation, much of the flow through the slot is supersonic.

References

[1]Delery, J. M., "Shock-Wave/Turbulent Boundary-Layer Interaction and Its Control," *Progress in Aerospace Sciences*, Vol. 22, No. 4, 1985, pp. 209–280.

[2]Hamed, A., and Shang, J., "Survey of Validation Data Base for Shock-Wave/Boundary-Layer Interactions in Supersonic Inlets," *Journal of Propulsion and Power*, Vol. 7, No. 4, 1991, pp. 617–625.

[3]Hamed, A., and Lehnig, T., "An Investigation of Oblique Shock/Boundary-Layer/Bleed Interaction," *Journal of Propulsion and Power*, Vol. 8, No. 2, 1992, pp. 418–424.

[4]Hamed, A., Shih, S., and Yeuan, J. J., "A Parametric Study of Bleed in Shock/Boundary-Layer Interactions," AIAA Paper 93-0294, Jan. 1993.

[5]Hamed, A., Yeuan, J. J., and Shih, S., "An Investigation of Shock Wave/Turbulent Boundary-Layer Interaction with Bleed Through Normal and Slanted Holes," AIAA Paper 93-2155, June 1993.

[6]Hamed, A., Yeuan, J. J., and Shih, S., "Flow Characteristics in Boundary-Layer Bleed Slots with Plenum," AIAA Paper 95-0033, Jan. 1995.

[7]Hamed, A., Yeuan, J. J., and Shih, S., "An Investigation of Shock Wave/Turbulent Boundary-Layer Interaction with Bleed Through Slanted Slots," AIAA Paper 93-2992, July 1993.

[8]Hahn, T. O., Shih, T. I.-P., and Chyu, W. J., "Numerical Study of Shock-Wave/Boundary-Layer Interactions with Bleed," *AIAA Journal*, Vol. 31, No. 5, 1993, pp. 869–876.

[9]Rimlinger, M. J., Shih, T. I.-P., and Chyu, W. J., "Three-Dimensional Shock-Wave/Boundary-Layer Interactions with Bleed Through a Circular Hole," AIAA Paper 92-3084, July 1992.

[10]Chyu, W. J., Rimlinger, M. J., and Shih, T. I.-P., "Effects of Bleed-Hole Geometry and Plenum Pressure on Three-Dimensional Shock-Wave/Boundary-Layer/Bleed Interactions," AIAA Paper 93-3259, July 1993.

[11]Shih, T. I.-P., Rimlinger, M. J., and Chyu, W. J., "Three-Dimensional Shock-Wave/Boundary-Layer Interactions with Bleed," *AIAA Journal*, Vol. 31, No. 10, 1993, pp. 1819–1826.

[12]Rimlinger, M. J., Shih, T. I.-P., and Chyu, W. J., "Three-Dimensional Shock-Wave/Boundary-Layer Interactions with Bleed Through Multiple Holes," AIAA Paper 94-0313, Jan. 1994.

[13]Harloff, G. J., and Smith, G. E., "On Supersonic-Inlet Boundary-Layer Bleed Flow," AIAA Paper 95-0038, Jan. 1995.

[14]Porro, A. R., and Hingst, W. R., "Use of Surface Heat Transfer Measurements as a Flow Separation Diagnostic in a Two-Dimensional Reflected Oblique Shock/Turbulent Boundary-Layer Interaction," AIAA Paper 93-0775, Jan. 1993.

[15]Blumenthal, P. Z., "A PC Program for Estimating Measurement Uncertainty for Aeronautics Test Instrumentation," AIAA Paper 95-3072, July 1995.

[16]Bencic, T., "Experiences Using Pressure Sensitive Paint in NASA Lewis Research Center Propulsion Test Facilities," AIAA Paper 95-2831, July 1995.

[17]Bryer, D. W., and Pankhurst, R. C., *Pressure-Probe Methods for Determining Wind Speed and Flow Direction*, Her Majesty's Stationery Office, London, 1971, Chap. 2.

[18]Willis, B. P., Davis, D. O., and Hingst, W. R., "Flow Coefficient Behavior for Boundary-Layer Bleed Holes and Slots," AIAA Paper 95-0031, Jan. 1995.

[19]Davis, D. O., Willis, B. P., and Hingst, W. R., "Flowfield Measurements in a Slot-Bled Oblique Shock-Wave and Turbulent Boundary-Layer Interaction," AIAA Paper 95-0032, Jan. 1995.

[20]Coleman, H. W., and Steele, W. G., *Experimentation and Uncertainty Analysis for Engineers*, Wiley, New York, 1989, Chap. 4.